FULL PAPER

Dalton
www.rsc.org/dalton

Equilibria and dynamics of some aqueous peroxomolybdophosphate catalysts: a potentiometric and ^{31}P NMR spectroscopic study

Fabian Taube,[a] Ingegärd Andersson,[a] Sarah Angus-Dunne,[a] Andrea Bodor,[b] Imre Tóth[b] and Lage Pettersson*[a]

[a] *Department of Chemistry, Inorganic Chemistry, Umeå University, SE-901 87 Umeå, Sweden*
[b] *Department of Inorganic and Analytical Chemistry, University of Debrecen, H-4010 Debrecen, Pf. 21, Hungary*

Received 17th January 2003, Accepted 15th April 2003
First published as an Advance Article on the web 8th May 2003

The equilibrium speciation in the $p\,H^+ + q\,MoO_4^{2-} + r\,H_2O_2 + s\,H_2PO_4^- + t\,SO_4^{2-} \rightleftharpoons (H^+)_p(MoO_4^{2-})_q(H_2O_2)_r(H_2PO_4^-)_s(SO_4^{2-})_t^{p-2q-s-2t}$ system in 0.300 M $Na_2(SO_4)$ medium at 25 °C and $[H_2O_2]_{tot}/[Mo]_{tot} > 2$ has been determined from potentiometric data and ^{31}P NMR integral and chemical shift data in the range $1.0 \le pH \le 9.0$, $2.0 \le [MoO_4^{2-}]_{tot}/mM \le 293$, $32 \le [H_2O_2]_{tot}/mM \le 640$, $2 \le [H_2PO_4^-]_{tot}/mM \le 60$ and $200 \le [SO_4^{2-}]_{tot}/mM \le 380$. Species with the following compositions were obtained: MoX_2P^{3-} (0,1,2,1,0), MoX_2P^{2-} (1,1,2,1,0), MoX_2P^- (2,1,2,1,0), $Mo_2X_4P^{3-}$ (2,2,4,1,0), $Mo_2X_4P^{2-}$ (3,2,4,1,0), $Mo_3X_6P^{3-}$ (4,3,6,1,0), $Mo_3X_6P^{2-}$ (5,3,6,1,0) and $Mo_4X_8P^{3-}$ (6,4,8,1,0). The numbers and charges of molybdenum (Mo), peroxide (X), phosphate (P) and sulfate (S) in each species are given in the abbreviated formula $Mo_qX_rP_sS_t^{p-2q-s-2t}$. The numbers in parentheses refer to the values of p, q, r, s and t in the formula above. The following formation constants with 3σ were obtained; $\log\beta_{0,1,2,1,0} = 5.16 \pm 0.09$, $\log\beta_{1,1,2,1,0} = 12.73 \pm 0.02$ ($pK_a = 7.63$), $\log\beta_{2,1,2,1,0} = 16.14 \pm 0.03$ ($pK_a = 3.42$), $\log\beta_{2,2,4,1,0} = 25.03$ (± 0.04), $\log\beta_{3,2,4,1,0} = 29.54 \pm 0.02$ ($pK_a = 4.51$), $\log\beta_{4,3,6,1,0} = 42.30 \pm 0.03$, $\log\beta_{5,3,6,1,0} = 44.06 \pm 0.08$ ($pK_a = 1.76$), $\log\beta_{6,4,8,1,0} = 57.30 \pm 0.07$. pK_a values for H_3PO_4 and $H_2PO_4^-$ were determined to 2.00 and 6.48, respectively. Chemical exchange processes were detected by ^{31}P NMR 2D EXSY and selective magnetisation transfer experiments between the complexes. An averaged lifetime, $\tau(X_2Mo–OP) \sim 30$ ms, can be estimated for the MoX_2P and Mo_2X_4P species at pH = 5.5 and 5 °C.

Introduction

Peroxometallates have a broad range of interesting properties; from biological activities, *e.g.* insulin mimicry[1,2] and their role in halide oxidising enzymes, such as chloroperoxidase,[3] to their catalytic properties in a wide variety of oxidative reactions.[4] Both peroxomolybdates and peroxotungstates are of interest due to their catalytic role in the epoxidation of alkenes and in the oxidation of alcohols by peroxide.[5–7]

It has been found that P- and As-containing compounds of the type $R_3[AO_4\{MO(O_2)_2\}_4]^{3-}$ where M = Mo, W; A = P, As and R is a bulky cation, *e.g.* $N(C_6H_{13})_4^+$, are also good catalysts for oxidative reactions by peroxide.[5] The first crystals of this type were isolated as the peroxotungstate, $((C_6H_{13})_4N)_3[PO_4\{WO(O_2)_2\}_4]$, by Venturello *et al.*[6] and subsequently crystals of $((C_6H_{13})_4N)_3[PO_4\{MoO(O_2)_2\}_4]$ have been isolated by Salles *et al.*[8] The anions of these were shown to epoxidise both 1-octene and (*R*)-(+)-limonene.[8] In both salts, each metal atom was found to contain one side-on bridging ($\eta^1;\eta^2$) and one side-on non-bridging (η^2) peroxo group. The presence of this peroxo moiety appears to be a key feature in the oxidative activity of these compounds.[9] Other peroxomolybdophosphates reported include the 2-aminopyridine salt of $[PO_4\{MoO(O_2)_2\}_4]^{3-}$[10] along with the structural characterisations of the mono- and bis-diperoxomolybdate species $[NH_4][(Ph_2PO_2)\{MoO(O_2)_2(H_2O)\}]$ and $[NMe_4][(Ph_2PO_2)\{MoO(O_2)_2\}_2]$[9] and the tris-diperoxomolybdate species $[NMe_4][(PhPO_3)\{MoO(O_2)_2\}_2\{MoO(O_2)_2(H_2O)\}]$.[11] The latter three species all show some catalytic activity for alkene epoxidation.

The highly selective delignification obtained in the bleach process of kraft pulp by peroxomolybdates under weakly acidic conditions[12–14] has proven to be more effective in the presence of phosphates.[15] In order to investigate the formation of possible peroxomolybdophosphates in the bleach process, a speciation and dynamic study of the $H^+–MoO_4^{2-}–H_2O_2–H_2PO_4^-$ system in 0.300 M $Na_2(SO_4)$ medium was performed by potentiometry and ^{31}P NMR spectroscopy at 5–25 °C, and excess of hydrogen peroxide ($[H_2O_2]_{tot}/[Mo]_{tot} > 2$). The study is based on earlier investigations of the $H^+–MoO_4^{2-}–SO_4^{2-}$[16] and the $H^+–MoO_4^{2-}–H_2O_2–SO_4^{2-}$[17] systems in the same medium. The sodium sulfate medium was chosen since Na^+ and SO_4^{2-} are the most common ions present in the bleach process.

Experimental

Chemicals and analyses

Molybdate stock solutions, sulfuric acid solutions and disodium sulfate were prepared according to ref. 16. Diluted solutions of hydrogen peroxide (E. Merck, 30%) were prepared according to ref. 17. Sodium dihydrogenphosphate monohydrate $NaH_2PO_4 \cdot H_2O$ (E. Merck *p.a.*) was without further purification, and solutions were standardised by evaporation at 120 °C and then weighed as anhydrous NaH_2PO_4. Diluted sodium hydroxide was prepared from a concentrated (50% H_2O and 50% NaOH) solution and standardised against sulfuric acid. The sodium hydroxide solutions were stored in plastic bottles. In all preparation of solutions, boiled distilled (Milli-Q plus 185) water was used. Alkaline and neutral solutions were protected from CO_2(g) by the use of argon gas.

Notation

The equilibria studied are written with the components H^+, MoO_4^{2-}, H_2O_2, $H_2PO_4^-$ and SO_4^{2-}. Species are formed according to:

$$p\,H^+ + q\,MoO_4^{2-} + r\,H_2O_2 + s\,H_2PO_4^- + t\,SO_4^{2-} \rightleftharpoons (H^+)_p(MoO_4^{2-})_q(H_2O_2)_r(H_2PO_4^-)_s(SO_4^{2-})_t^{p-2q-s-2t} \quad (1)$$

Formation constants are denoted $\beta_{p,q,r,s,t}$, and the stoichiometry of each species are either given by the notation (p,q,r,s,t), or by the abbreviated formula $Mo_qX_rP_sS_t^{p-2q-s-2t}$, where (Mo) corresponds to MoO_4^{2-}, (X) to the peroxo ligand, (P) to $H_2PO_4^-$ and (S) to SO_4^{2-}. In case where the sum of protonation steps for a species is given, the charge has been omitted. The total concentrations of molybdate, hydrogen

DOI: 10.1039/b300702b

peroxide, phosphate and sulfate are denoted $[Mo]_{tot}$, $[P]_{tot}$, $[H_2O_2]_{tot}$ and $[S]_{tot}$, respectively. The study has been performed in 0.300 M sodium sulfate medium with the cation concentration kept constant. Therefore, the medium is denoted $Na_2(SO_4)$ implying that $[Na^+]$ has been kept constant 0.600 M.

Preparation and equilibration of solutions

To avoid decomposition of peroxide in the solutions during preparation and titration, certain procedures had to be followed. Since the decomposition of peroxide in most solutions is expected to increase noticeably at pH around 5.5 and higher,[17] the sulfuric acid was always added prior to the addition of hydrogen peroxide during the preparation of each solution. The solutions were then allowed to equilibrate for about 20 min before starting the titration. All solutions containing peroxide were prepared and titrated in black glass equipment.

Potentiometric measurements

The measurements were carried out in 0.300 M $Na_2(SO_4)$ medium at 25 °C using potentiometric titrations as described in ref. 16. For the H^+– MoO_4^{2-}–H_2O_2–$H_2PO_4^-$–SO_4^{2-} system, most solutions were prepared to pH ~ 2 and titrated with a sodium hydroxide solution, or an alkaline phosphate solution, having the proper medium conditions. These titrations were stopped at pH around 6. In some titrations the pH value was kept almost constant, changing only the $[Mo]_{tot}/[P]_{tot}$ ratio.

Potentiometric data

The potentiometric data include 187 experimental points, within $20 \le [Mo]_{tot}/mM \le 160$, $80 \le [H_2O_2]_{tot}/mM \le 640$, $10 \le [P]_{tot}/mM \le 60$ and $200 \le [S]_{tot}/mM \le 300$. For the H^+–$H_2PO_4^-$ subsystem, potentiometric data including 225 experimental points within $10 \le [P]_{tot}/mM \le 60$ and pH 2.0–9.0 was used in the calculations. For pH determination of the NMR solutions, an Ingold U402-M6-S7/100 combination electrode was used and calibrated against buffer solutions of known $[H^+]$. Thus, the pH measurements are on a concentration scale, where $-\log [H^+] = pH$.

NMR measurements

^{31}P NMR spectra were recorded at 145.8 and 202.5 MHz on a Bruker AM 360 and AMX 500 MHz spectrometer, respectively, at 5 and 25 (±1) °C. Field-frequency stabilization was achieved by placing the 8 mm sample tube into a 10 mm tube containing D_2O (for Bruker AMX 500) or by adding 10% D_2O to the sample tubes (for Bruker AM 360). All chemical shifts are reported relative to the external reference 85% H_3PO_4, assigned to 0 ppm. Typically, spectral widths of 10 ppm (2 kHz) were used, and data for the FID were accumulated in 32k blocks. Using a 30° pulse and 4 s relaxation delays (Bruker AM 360 MHz) or a 90° pulse and 35 s relaxation delays (AMX 500 MHz), quantitative integration could be done. Exponential line broadening (1 Hz) was applied before Fourier transformation. Spectra were quantitatively integrated after baseline correction. The deconvolution subroutine of the software program 1D WINNMR was used for precise integral evaluation.

NMR integral and chemical shift data

For the H^+–MoO_4^{2-}–H_2O_2–$H_2PO_4^-$–SO_4^{2-} system, the pH value was measured on an aliquot of the sample concurrently with each ^{31}P NMR measurement. Many samples consisted of solutions, which were extracted from the vessel solution during the titrations. Owing to the increased decomposition of H_2O_2 above pH ~5.5, ^{31}P NMR measurements on solutions in the pH range 5–6 were made within 1 h after preparation. For chemical shift data, the pH range was expanded to 1.0–8.1. However, in the pH range 6.0–8.1 equilibrium was not reached due to decomposition of peroxide. These data were only used for pK_a determinations. ^{31}P NMR integral data from 112, and chemical shift data from 143 spectra in the ranges $1.0 \le pH \le 8.1$, $2.0 \le [Mo]_{tot}/mM \le 293$, $32 \le [H_2O_2]_{tot}/mM \le 783$, $2.0 \le [P]_{tot}/mM \le 60$, $220 \le [S]_{tot}/mM \le 380$ were used. For the H^+–$H_2PO_4^-$ subsystem, chemical shift data from 51 spectra in the ranges $10.0 \le [P]_{tot}/mM \le 60$, pH 0.2–9.7 were collected and used in the calculations.

Evaluation of equilibrium constants

The potentiometric data and the quantitative ^{31}P NMR data (integral and chemical shift) were evaluated using the least squares program LAKE.[18] The LAKE program is able to calculate formation constants from a combination of different kinds of data. In the program, formation constants for arbitrary but systematically chosen species $(H^+)_p(MoO_4^{2-})_q(H_2O_2)_r(H_2PO_4^-)_s(SO_4^{2-})_t^{p-2q-s-2t}$ are varied, so that the sum of error squares, $U = \Sigma(W_i \Delta A_i)^2$, is minimized. The set of species giving the lowest U-value forms the model, which best explains the experimental data. A_i can be either the total concentration of components, concentration of species, NMR integrals or chemical shifts. W_i is a weighting factor for the different types of data. In this study we have used a weighting factor that gives NMR integrals a predominant contribution to the sum of residuals. Modelling and construction of distribution diagrams were performed using the program SOLGASWATER.[19]

Dynamic NMR studies

Both spin–spin (T_2) and spin-lattice relaxation time scales (T_1) could be used to follow the dynamics in this system. Line width data of signals found in the 'slow exchange regime' on the actual chemical shift time scale were evaluated by fitting Lorentz-curves. Line broadening (LB in Hz) of the ^{31}P NMR signals, due to chemical exchange, was calculated as $LB = LW^{obs} - LW^0$, where LW^{obs} is the observed line width, and LW^0 is the non-exchange line width of the signal, respectively. For all exchanging sites in ^{31}P NMR, $LW^0 \approx 10$ Hz was estimated from low temperature experiments. This value is significantly larger than the usual line width for the half spin ^{31}P nucleus, probably because of the paramagnetism of O_2 formed from the slow decomposition of H_2O_2 in the samples. The pseudo-first order rate constants were calculated by using the formula $k_{obs} = LB \cdot \pi$.[20]

Magnetization transfer (MT) experiments were done by the simplest rectangular shaped Dante sequence with typically 30–50 pieces, 1–1.2 μs long pulses applying *ca.* 0.5 ms delays in between. The total pulse length and the selectivity were roughly calculated and then tuned experimentally, usually achieving 85–95% efficiency for inversion.The change in magnetization vector (taken from the integrated intensity of the corresponding signal) is given by:

$$\boldsymbol{M}_t = \exp(\boldsymbol{R} \cdot t) \cdot (\boldsymbol{M}_0 - \boldsymbol{M}_\infty) + \boldsymbol{M}_\infty \qquad (2)$$

where $\boldsymbol{M}$ is the column matrix of magnetization on each site at time t, $\boldsymbol{M}_\infty$ is the column matrix of equilibrium longitudinal magnetization. $\boldsymbol{R}$ is the square rate matrix with off-diagonal elements, $\boldsymbol{R}_{ij} = k_{ji}$ (the pseudo–first order rate constant from site j to site i), and diagonal elements;

$$\boldsymbol{R}_{ij(i=j)} = -\frac{1}{T_{1i}} - \sum_{i \neq j} k_{ji} \qquad (3)$$

The unknown parameters $\boldsymbol{M}_\infty$, T_{1i}, k_{ji} have been fitted with a non-linear least-squares method using the MATLAB program.

^{31}P NMR 2D EXSY spectra were also recorded for the system. The classical NOESY pulse program from Bruker was used.

Table 1 Species, formation constants and ^{31}P NMR chemical shifts for the H^+–$H_2PO_4^-$ and H^+–MoO_4^{2-}–H_2O_2–$H_2PO_4^-$ systems in 0.300 M $Na_2(SO_4)$ medium at 25 °C and excess of peroxide ($[H_2O_2]_{tot}/[Mo]_{tot}$ > 2). Potentiometric titration data in the pH range 2.0–6.0 and ^{31}P NMR integral and chemical shift data in the pH range 1.0–8.1 (peroxomolybdophosphate system) and 0.2–9.7 (phosphate system) have been used; 3σ error limits are given in parentheses

(*p*,*q*,*r*,*s*)	Notation	log*β*	pK_a	δ_P/ppm
−1,0,0,1	P^{2-}	−6.483(6)		3.22(1)
0,0,0,1	P^-	0	6.48	0.67(1)
1,0,0,1	P	2.00(1)	2.00	0.46(2)
0,1,2,1	MoX_2P^{3-}	5.16(9)		7.86(22)
1,1,2,1	MoX_2P^{2-}	12.73(2)	7.57	2.84(3)
2,1,2,1	MoX_2P^-	16.14(3)	3.41	1.30(4)
2,2,4,1	$Mo_2X_4P^{3-}$	25.03(4)		4.76(3)
3,2,4,1	$Mo_2X_4P^{2-}$	29.54(2)	4.51	2.40(2)
4,3,6,1	$Mo_3X_6P^{3-}$	42.30(3)		3.90(3)
5,3,6,1	$Mo_3X_6P^{2-}$	44.06(8)	1.76	2.75(12)
6,4,8,1	$Mo_4X_8P^{3-}$	57.30(7)		3.42

Results and discussion

Equilibrium calculations

Subsystems. To establish the speciation in the five component H^+–MoO_4^{2-}–H_2O_2–$H_2PO_4^-$–SO_4^{2-} system, the equilibrium constants for the subsystems must be accurately known under the same experimental conditions (*i.e.* same temperature and ionic medium). The sulfate,[16] molybdate[16] and peroxomolybdate[17] constants have been determined earlier in 0.300 M $Na_2(SO_4)$ medium at 25 °C. In the present study an excess of peroxide ($[H_2O_2]_{tot}/[Mo]_{tot}$ > 2) has been used to resemble the conditions in the industrial process. From the ^{31}P NMR measurements, it was discerned that no molybdophosphate species, MoP, were formed. Instead, monophosphate species, P, were present, as shown in Fig. 1. Therefore, constants in the H^+–$H_2PO_4^-$ system had to be determined. The formation constants and chemical shifts obtained are given in Table 1. Addition of H_2O_2 had no effect on this system, *i.e.* peroxophosphate species were not formed under the present conditions. The table has been simplified by excluding the SO_4^{2-} component because no peroxomolybdophosphate species containing sulfate could be identified.

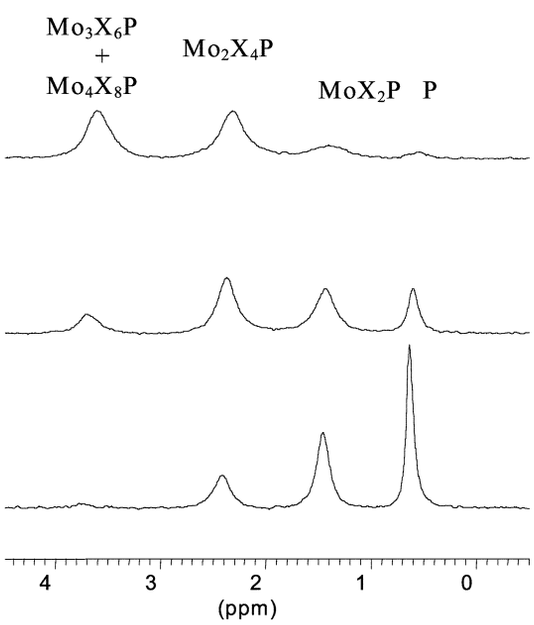

Fig. 1 ^{31}P NMR spectra of three solutions at pH ~ 2.5. $[Mo]_{tot}/[H_2O_2]_{tot}/[P]_{tot}$ from top to bottom: 160/480/20, 80/240/20, 40/120/20 mM.

The peroxomolybdophosphate system. In Fig. 1, showing three ^{31}P NMR spectra at $[H_2O_2]_{tot}/[Mo]_{tot}$ = 3 (pH ~ 2.5) and $[Mo]_{tot}/[P]_{tot}$ = 8 (top), 4, and 2 (bottom), three signals arising from peroxomolybdophosphates can be discerned. The signal to the left was found to be a sum of two overlapping signals, originating from species having the highest $[Mo]_{tot}/[P]_{tot}$ ratio, *i.e.* Mo_3X_6P and Mo_4X_8P. The other two signals were found to originate from Mo_2X_4P and MoX_2P species, respectively. As can be seen from the spectra, the coordination of phosphate to peroxomolybdates is weak and an appreciable amount of monomeric phosphate, P, is present even at $[Mo]_{tot}/[P]_{tot}$ = 8. At $[Mo]_{tot}/[P]_{tot}$ ~20, the signal originating from the Mo_4X_8P species could be discerned, but due to severe overlapping of the signals at 25 °C, signals could only be deconvoluted in the pH range ≤1.5. However, at 5 °C the chemical exchange is slower and the signal is well separated even at higher pH values (Fig. 2). In contrast to the other signals, which are all shifted upfield upon protonation, the shift of this signal was not affected by the pH value in solution, implying that the oxygens around the phosphorous atom are not protonated. If the structure of $Mo_4X_8P^{3-}$ in solution corresponds to the structure found by Salles *et al.*[8] in the solid phase, then all four phosphate oxygens are coordinated to molybdenum atoms and are therefore not likely to be protonated.

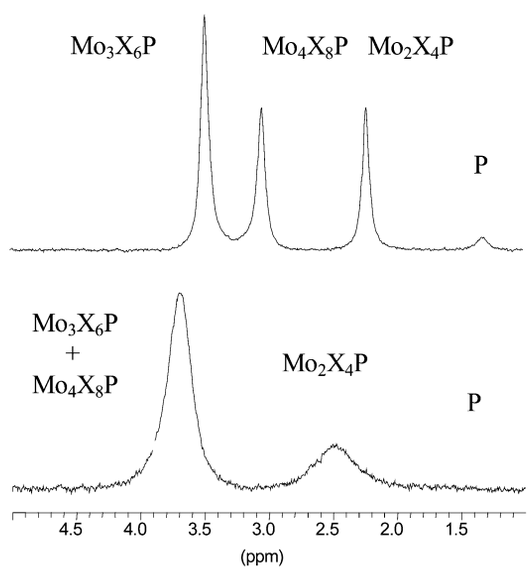

Fig. 2 ^{31}P NMR spectra at 5 °C, pH 2.29 (upper) and at 25 °C, pH 2.38 (lower). $[Mo]_{tot}$ = 293 mM, $[H_2O_2]_{tot}$ = 783 mM, $[P]_{tot}$ = 15 mM and $[S]_{tot}$ = 205 mM.

Fig. 3 illustrates the ^{31}P chemical shifts as a function of pH for all the MoX_2P^{n-} (n = 1, 2, 3), $Mo_2X_4P^{n-}$ (n = 2, 3), $Mo_3X_6P^{n-}$ (n = 2, 3) and $Mo_4X_8P^{n-}$ (n = 3) species and also for the monophosphate species, P^{n-} (n = 0–2). Such a plot shows the pH range of existence for each species and also indicates which species that undergo protonation. For equilibrium calculations, experimental data points from potentiometric titrations and ^{31}P NMR integral data in the pH-range 0.9–6.0 have been used. However, in order to determine the pK_a value of MoX_2P^{2-}, the pH-range for chemical shift data was increased to 8.1.

It should be noticed that the equilibrium study in the H^+–MoO_4^{2-}–H_2O_2–SO_4^{2-}subsystem is investigated only for pH values down to 2.0 and molybdate concentration up to 80 mM.[17] In that study, a protonation of the dimeric $Mo_2X_4^{2-}$ (2,2,4,0) species was suggested, but could not be confirmed by potentiometry due to the moderate concentration of molybdate used in the titrations. In the present study, where molybdate concentration up to 293 mM has been used, this $Mo_2X_4^-$ (3,2,4,0) species might play an important role. Therefore, additional titrations at high molybdate concentrations were

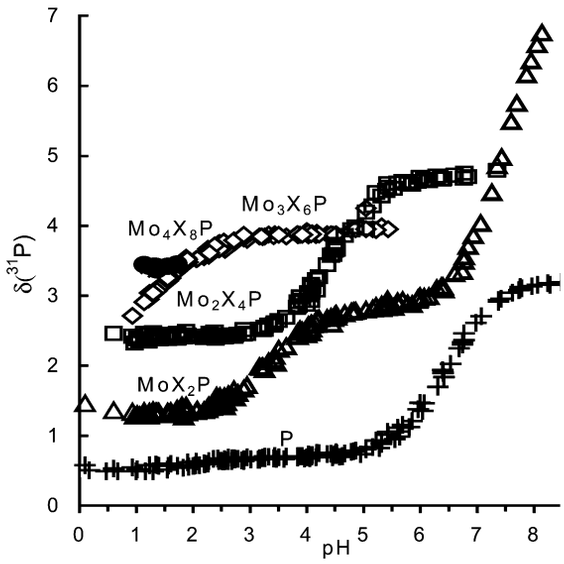

Fig. 3 ^{31}P NMR chemical shifts as a function of pH. The symbols represent experimental NMR points.

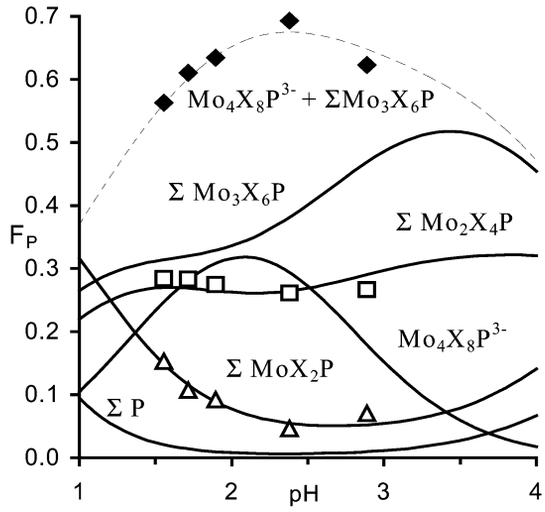

Fig. 5 Distribution of phosphate, F_P, as a function of pH at $[Mo]_{tot}$ = 293 mM, $[H_2O_2]_{tot}$ = 783 mM, $[P]_{tot}$ = 15 mM and $[S]_{tot}$ = 260 mM. The symbols represent experimental NMR points. The full curves have been calculated using the model given in Table 1 and the subsystems.[16,17]

performed in the H^+–MoO_4^{2-}–H_2O_2–SO_4^{2-}subsystem. From the equilibrium calculations, the formation constant, $\log\beta_{3,2,4,0}$, was found to be 26.0 (pK_a = 2.1). The $\log\beta_{3,2,4,0}$ constant was then used as a fixed constant for the calculations in the H^+–MoO_4^{2-}–H_2O_2–$H_2PO_4^-$–SO_4^{2-} system.

Using the formation constant for $Mo_2X_4^-$, the formation constants for the subsystems obtained earlier,[16,17] and the constants compiled in Table 1, distribution diagrams have been constructed. Since each ^{31}P NMR signal represents the sum of species with the same nuclearity that are in rapid exchange on the NMR time scale, rather than individual protonated/deprotonated species, the distribution diagram has been constructed to show the sum of such species. From the distribution of phosphate (F_P) at $[Mo]_{tot}/[P]_{tot}$ = 4 in Fig. 4, it can be seen that species with $[Mo]_{tot}/[P]_{tot}$ ratios of 2 and below, *i.e.* MoX_2P^{n-} and $Mo_2X_4P^{n-}$, predominate over almost the entire pH range (the fractional proportion of $Mo_4X_8P^{3-}$ is less than 0.05 and has been excluded in the figure). Only at relatively high $[Mo]_{tot}/[P]_{tot}$ ratios does $Mo_3X_6P^{n-}$ predominate, as illustrated in Fig. 5 at $[Mo]_{tot}/[P]_{tot}$ = 19.5. Here, one of the signals represents the sum of both $Mo_3X_6P^{n-}$ (n = 2, 3) and $Mo_4X_8P^{3-}$. This sum is modelled as a dashed line, together with the experimental NMR integral data.

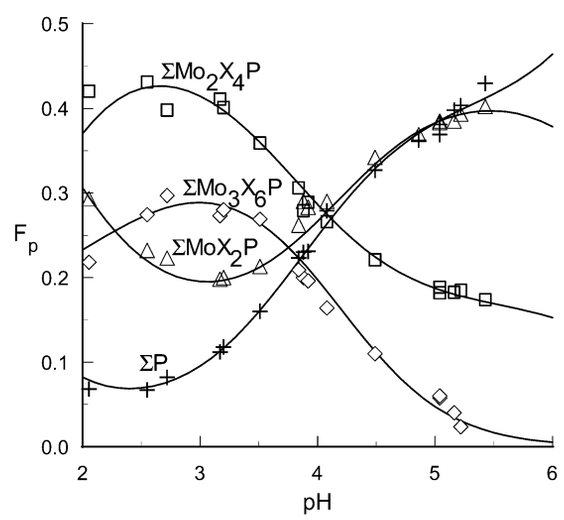

Fig. 4 Distribution of phosphate, F_P, as a function of pH at $[Mo]_{tot}$ = 160 mM, $[P]_{tot}$ = 40 mM, $[H_2O_2]_{tot}$ = 490 mM and $[S]_{tot}$ = 200 mM. F_P is defined as the ratio between [P] in a given species and $[P]_{tot}$ in solution. The symbols represent experimental NMR points. The full curves have been calculated using the model given in Table 1 and the subsystems.[16,17]

The distribution of P- and Mo-containing species is illustrated in Fig. 6. Because ordinary F_P and F_{Mo} diagrams become too complex, the distribution is shown as cumulative α_P and α_{Mo} diagrams. Each species is represented by an area, and its fraction, α_P andα_{Mo}, at a given pH is the vertical height of its area at that pH. These diagrams have, similar to Fig. 4, been calculated for $[P]_{tot}$ = 40 mM and excess of hydrogen peroxide ($[Mo]_{tot}/[H_2O_2]_{tot}$ = 3), but at $[Mo]_{tot}/[P]_{tot}$ = 2. At these concentrations a substantial amount of P is present as monomeric phosphate (Fig. 6(a)). The Mo-distribution (Fig. 6b) shows that only *ca.* 25% (pH 6) to *ca.* 50% (pH 2) of Mo is bound in peroxomolybdophosphate species. Substantial amounts are bound in diperoxomonomolybdate and tetraperoxodimolybdate species, and at low pH also in the diperoxomonomolybdosulfate species, MoX_2S^{2-}.

Given the concentrations found in the bleach process, *i.e.* up to 1 mM of molybdate, 0.5 mM of phosphate and large excess of peroxide, MoX_2P^{n-} seems to be the only peroxomolybdophosphate species of importance, as illustrated in Fig. 7(a)). As can be seen in Fig. 7(b), this is however a very minor species, compared to both the MoX_2 species and the MoX_2S^{2-} species.

Equilibrium dynamics

As can be seen from Fig. 1, the line widths of the different signals are dependent on the concentration of the species, *i.e.* the population of the ^{31}P site in the species giving rise to the signal. There is also a temperature dependence of the line widths, and from Fig. 2 it can be concluded that the chemical exchange between species with different nuclearities is in the slow exchange regime at 5 °C and pH ~2.3, but not at 25 °C. However, the three-site exchange system involving P, MoX_2P and Mo_2X_4P can be resolved at 25 °C.[21]

The exchange broadening is substantial for the less populated sites, such as the ^{31}P sites in the MoX_2P and P species (top spectra in Fig. 1), and close to the detection limit (≈5 Hz) for the major species. In order to trace the exchange reaction paths between the different species, 2D EXSY and selective magnetisation transfer (MT) experiments have been carried out. In Fig. 8, 2D EXSY spectra at two different mixing times, τ_m, are shown. At τ_m = 15 ms (top), there are cross-peaks between MoX_2P and free phosphate, P, and MoX_2P and Mo_2X_4P, but there is no detectable cross-peak between P and Mo_2X_4P. However, at τ_m = 30 ms (bottom) all cross-peaks are clearly visible.

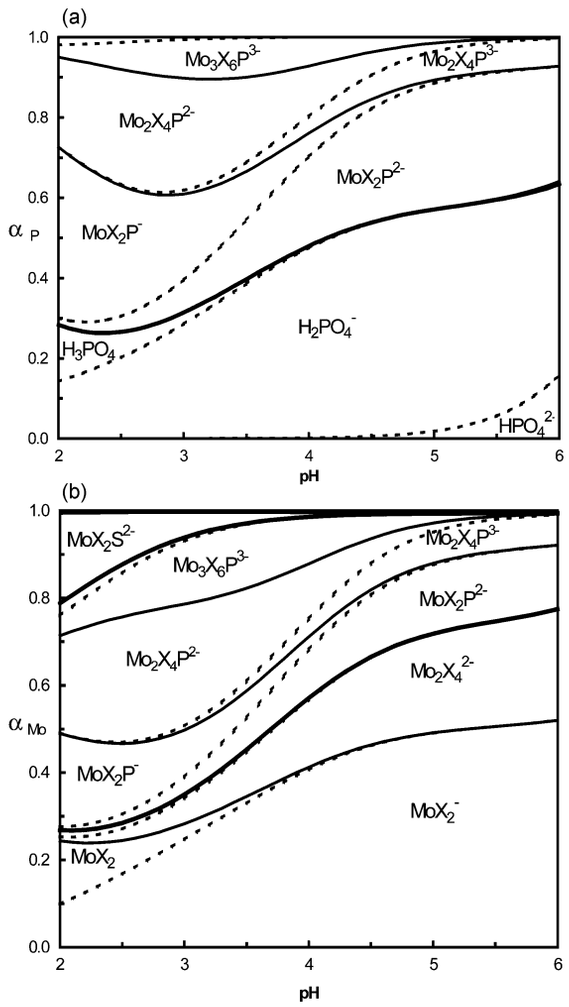

Fig. 6 Diagrams showing the cumulative distribution of (a) phosphate- and (b) molybdate-containing species as a function of pH at $[Mo]_{tot}$ = 80 mM, $[H_2O_2]_{tot}$ = 240 mM, $[P]_{tot}$ = 40 mM and $[S]_{tot}$ = 300 mM. Each species is represented by an area and its fraction at a given pH is the vertical height of its area at that pH. Full lines separate species with different nuclearities, and dashed curves species in proton series.

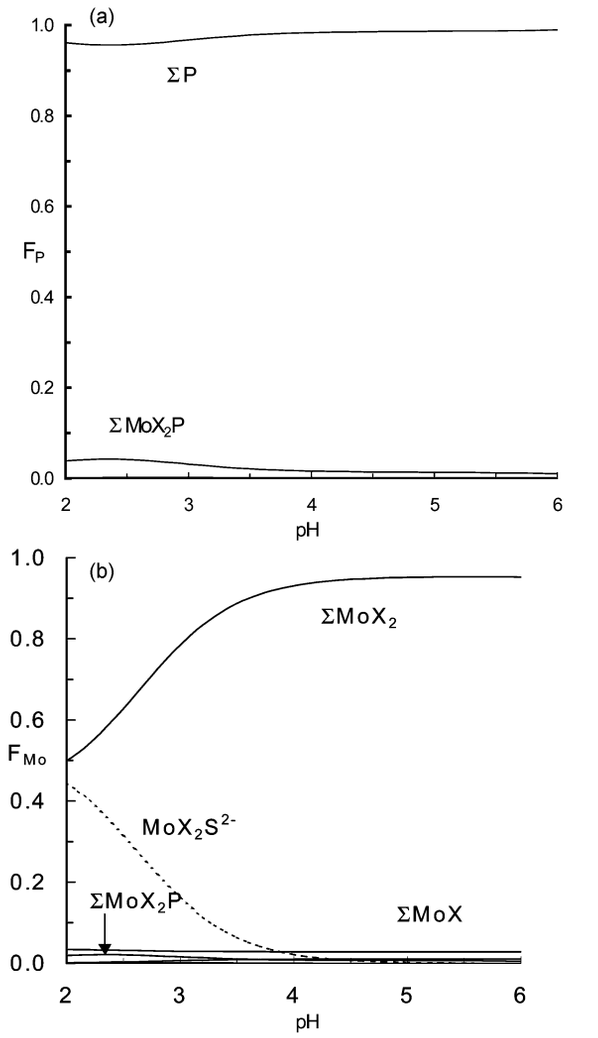

Fig. 7 Diagrams showing the distribution of (a) phosphate and (b) molybdate as a function of pH at $[Mo]_{tot}$ = 1 mM, $[P]_{tot}$ = 0.5 mM, $[H_2O_2]_{tot}$ = 30 mM and $[S]_{tot}$ = 300 mM.

This observation can be interpreted in two ways. Either (i) the chemical exchange between MoX_2P and P and MoX_2P and Mo_2X_4P are substantially faster than the exchange between free phosphate and Mo_2X_4P, because the latter cannot be detected at 15 ms mixing time. Or (ii) the cross-peaks measured at 30 ms between free phosphate and Mo_2X_4P may be attributed to indirect exchange, *i.e.* the exchange goes through MoX_2P, this being in exchange with both the other species. This explanation seems to be the most rational from structural point of view, because it requires only one MoX_2 unit to be added or subtracted in one elementary step.

By the use of MT, it is possible to elucidate the "direct" chemical exchange between the different species. Fig. 9 shows that the negative magnetization from the excited MoX_2P is transferred to Mo_2X_4P and P immediately (some transfer even happens during the time required for the DANTE pulse train, see symbols at 0.001 s). As can be seen, the transfer of the excitation is almost equally fast to both Mo_2X_4P and P. The intensities are changing until somewhere between 0.01 and 0.05 s, and then become steady until nearly 1 s. In other words, the intensities in this delay time region are controlled by the chemical exchange processes (the spin lattice relaxation, T_1, is negligible here). At delay time longer than 1 s, T_1 becomes dominant, and at 15–20 s the relaxation is complete. In another experiment, in which P was labelled with negative magnetization, a similar decrease in intensity was noted for MoX_2P, but not for the intensity of the Mo_2X_4P signal. This implies that there is no direct exchange between free phosphate and Mo_2X_4P.

A quantitative evaluation of the MT experiments resulted in the following model:

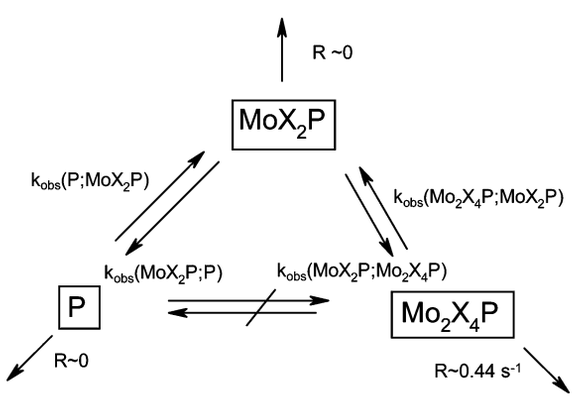

The computed pseudo-first-order rate constants for the active exchange paths are: $k_{obs}(MoX_2P;P) = 39 \pm 5\ s^{-1}$, $k_{obs}(P;MoX_2P) = 84 \pm 11\ s^{-1}$ and $k_{obs}(MoX_2P;Mo_2X_4P) = 33 \pm 3\ s^{-1}$, $k_{obs}(Mo_2X_4P;MoX_2P) = 32 \pm 3\ s^{-1}$. The rate of spin-lattice relaxation, $R = 1/T_1$, is calculated to 0.44 s^{-1}. The site for relaxation cannot be deduced unequivocally from this experiment, but is either Mo_2X_4P or MoX_2P.[22]

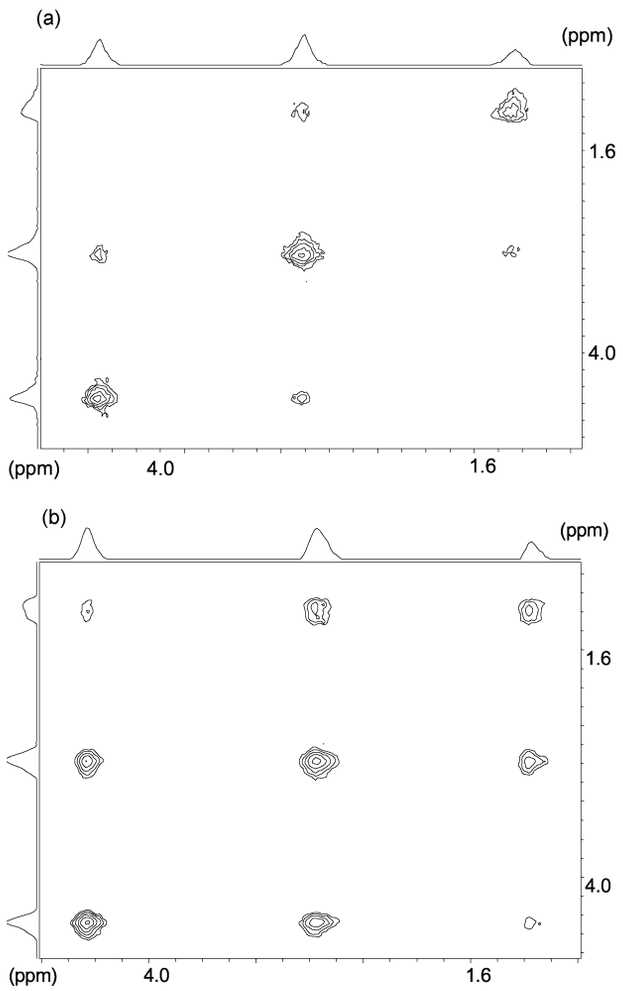

Fig. 8 ^{31}P NMR 2D EXSY spectra recorded at 25 °C in a sample with $[Mo]_{tot}$ = 600 mM, $[P]_{tot}$ = 150 mM, $[H_2O_2]_{tot}$ = 1800 mM and pH ~5.6: (a) τ_m = 15 ms, (b) τ_m = 30 ms.

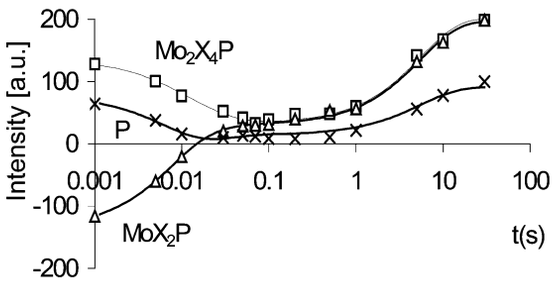

Fig. 9 Intensity (arbitrary units) *vs.* delay time of a ^{31}P NMR selective magnetization transfer experiment at 25 °C and pH ~5.5: $[Mo]_{tot}$ = 600 mM, $[P]_{tot}$ = 150 mM, $[H_2O_2]_{tot}$ = 1800 mM. MoX_2P has been selectively excited. The symbols represent experimental values and the lines are calculated using a model including all rate constants.

In order to elucidate the lifetime of the exchanging part of the molecules, a comparison between some of the rate constant can be made. Because the P–O bond is considered to be very inert, the calculated lifetime is that of the Mo–O bond, *i.e.* the $–O–MoX_2$ unit. For example, the exchange between MoX_2P and P, $k_{obs}(MoX_2P;P)$, and between MoX_2P and Mo_2X_4P, k_{obs}-$(Mo_2X_4P;MoX_2P)$, can be attributed to the leaving of one $X_2Mo–$ unit from a $X_2Mo–OP$ entity. Thus, the lifetime of the $X_2Mo–OP$ entity in the two different species, $\tau(Mo–OP) = 1/k_{obs}$ ~26 ± 3 ms and 31 ± 2 ms, respectively, is similar. In our earlier paper,[23] a 7 ms lifetime has been attributed to the –Mo=O entity in the dimeric Mo_2X_4 species. It means that the lifetime of the Mo–O–(Mo) bond is substantially shorter compared to the lifetime for the Mo–(OP) bond measured in this work. However, both constants are conditional lifetime values, measured at different pH values (2.2 and 5.6).

Concluding remarks

The speciation study of the peroxomolybdophosphate system has given a wider insight into a system of pronounced interest for catalysis. It has shown that peroxomolybdophosphate species are minor compared to peroxomolybdate species under the conditions used in this study. Also, it can be concluded that the catalytically active $Mo_4X_8P^{3-}$ species[8,9] most likely is absent in the bleach process and that MoX_2P^{n-} seems to be the only peroxomolybdophosphate species of importance. From the dynamic study it can be concluded that the species found are in chemical exchange. However, there is no direct chemical exchange between free phosphate and Mo_2X_4P. Furthermore, the lifetime of the Mo–(OP) bond measured in this work was found to be substantially longer than the lifetime of the Mo–O–(Mo) bond, measured in our previous work.[23] This multi-component system is quite complex and interesting both from equilibrium and dynamic point of view, and further kinetic studies are under progress to explore the detailed kinetics in the system.

Acknowledgements

This work has been financially supported by The Strategic Foundation (SSF), the Swedish Natural Science Research Council (NFR), the European Union (COST project D12/0027-99) and the Hungarian Science Research Foundation (OTKA T 038296). We would like to thank Dr Oliver Howarth for valuable comments and linguistic corrections.

References

1 J. Wijkander, L. S. Holst, T. Rahn and S. Resjö, *J. Biol. Chem.*, 1997, **272**, 21520.
2 B. I. Posner, R. Faure, J. W. Burgess, A. P. Bevan and D. Lachance, *J. Biol. Chem.*, 1994, **269**, 4596.
3 A. Messerschmidt and R. Wever, *Proc. Natl. Acad. Sci. USA*, 1996, **93**, 392.
4 S. Sakaue, Y. Sakata, Y. Nishiyama and Y. Ishii, *Chem. Lett.*, 1992, **2**, 289.
5 A. C. Dengel, W. P. Griffith and B. C. Parkin, *J. Chem. Soc., Dalton Trans.*, 1993, 2683.
6 C. Venturello, R. D'Aloiso, J. C. J. Bart and M. Ricci, *J. Mol. Catal.*, 1985, **32**, 107.
7 N. J. Campbell, A. C. Dengel, C. J. Edwards and W. P. Griffith, *J. Chem. Soc., Dalton Trans.*, 1989, 1203.
8 L. Salles, C. Aubry, F. Robert, G. Chottard, R. Thouvenot, H. Ledon and J-M. Bregault, *New J. Chem.*, 1993, **17**, 367.
9 N. M. Gresley, W. P. Griffith, B. C. Parkin, A. J. P. White and D. J. Williams, *J. Chem. Soc., Dalton Trans.*, 1996, 2039.
10 R. G. Beiles, Z. E. Rozmanova and O. B. Andreeva, *Russ. J. Chem.*, 1969, **14**, 1122.
11 W. P. Griffith, B. C. Parkin, A. J. P. White and D. J. Williams, *J. Chem. Soc., Dalton Trans.*, 1995, 3131.
12 R. Agnemo, *9th ISWPC, Montréal, Canada*, ISBN 1-896742-14-9, 1997, D2-1.
13 V. Kubelka, R. C. Francis and C. W. Dence, *J. Pulp Pap. Sci.*, 1992, **18**, J108.
14 J. Jakara, A. Paren, J. Patola and T. Viitanen, *Pap. Puu.*, 1994, **76**, 559.
15 R. Agnemo, personal communication.
16 F. Taube, I. Andersson and L. Pettersson, *Polyoxometalates: From Topology to Industrial Applications*, ed. M. T. Pope and A. Müller, Kluwer Academic Publishers, 2001, pp. 161—174.
17 F. Taube, M. Hashimoto, I. Andersson and L. Pettersson, *J. Chem. Soc., Dalton Trans.*, 2002, 1002.
18 I. Ingri, I. Andersson, L. Pettersson, A. Yagasaki, L. Andersson and K. Holmström, *Acta Chem. Scand.*, 1996, **50**, 717.
19 G. Eriksson, *Anal. Chim. Acta.*, 1979, **112**, 375.
20 J. Sandström, *Dynamic NMR Spectroscopy*, Academic Press, London, 1982, p. 17.

21 The proton exchange – which is in fact ^{31}P exchange – between the differently protonated forms is fast, resulting in time averaged signals of a given species. The pH dependence of the chemical shift (Fig. 3) could therefore be used to evaluate the protonation constants.
22 There are two governing processes, the chemical exchange, and the relaxation. After 1 s the relaxation becomes dominant. This does not mean that the estimated relaxation time is 1 s. On the other hand, the calculated rate of spin–lattice relaxation $R = 1/T_1 = 0.44\ s^{-1}$. From this expression the value of $T_1 = 2.3$ s. This is in full accordance with Fig. 9, as complete relaxation is achieved after about $5 \times T_1 = 12$ s. Calculation and evaluation of T_2 is out of the scope of this work. The existence of paramagnetic O_2 in solution opens new routes for relaxation (quadrupolar relaxation) having an effect on both T_1 and T_2 values. We considered the line width of 10 Hz measured at low temperatures as the non-exchange value, and this is in accordance with our kinetic calculations.
23 F. Taube, I. Andersson, I. Toth, A. Bodor, O. Howarth and L. Pettersson, *J. Chem. Soc., Dalton Trans.*, 2002, 4451.